Longitudinal Strength and Stiffness of Corrugated Steel Pipe

BRIAN T. HAVENS, F. WAYNE KLAIBER, ROBERT A. LOHNES, AND LOREN W. ZACHARY

Iowa, as well as other states, has experienced several failures of corrugated metal (CMP) culverts, apparently because of inlet flotation. In Iowa, most of these failures have occurred on secondary roads. In a survey of Iowa county engineers, 31 CMP culvert failures occurred within a 5-year period (1983 to 1988). A survey of state departments of transportation revealed nine CMP failures within the 5 years preceding 1992. Design standards from various states for tiedowns to resist uplift showed resisting forces ranging from 44.5 kN (10 kips) to 293.7 kN (66 kips) for pipes 2.03 m (80 in.) in diameter. Data from the survey of states verified an earlier conclusion based on responses from Iowa county engineers that when end restraint is not provided, there is a potential for uplift failures. Further, standards for existing restraint systems have an unclear theoretical or experimental basis, or both. Discussed here is the initial phase of a research program at Iowa State University, where a design procedure is being developed to determine the necessity and magnitude of restraining force to prevent CMP uplift failures. Theoretical relationships were developed for predicting the longitudinal stiffness, yield moment capacity, and ultimate moment capacity of CMP. Full-scale tests of steel CMPs 1.22 m (4 ft) and 1.83 m (6 ft) in diameter experimentally determined EI factors of 2.49 MN-m^2 (869×10^6 in^2-lb) and 2.61×10^6 N-m^2 (911×10^6 in^2-lb), respectively (3×1 corrugation style). The agreement of theoretical and experimental results verifies the accuracy of the theoretical relationships which will be used in the development of rational design standards.

Corrugated metal pipes (CMP) often serve as an inexpensive means for crossing small streams and thus are important components in the transportation system. Iowa, as well as other states in recent years, has experienced several CMP failures because of inlet flotation. Analytical design procedures in use today frequently overlook or underestimate the possibility of longitudinal flexural failures which may result from uneven settlement beneath the CMP or inlet uplift because of pore water pressure. Pressure beneath the inlet may be caused by a hydraulic head differential between the CMP inlet and outlet, by high storm flows, or by partial or full blockage of the inlet (*1*). The uplift can be aggravated by a small amount of water in the CMP, by minimum soil cover on the CMP, or by ineffective seepage cut-off below the inlet. Pore pressures can cause the inlet end of the CMP to deflect upward, which will result in longitudinal bending; longitudinal bends up to 90 degrees will often lead to erosion of the soil and roadway above the CMP (*2*). In some situations, the entire CMP may be dislodged from its existing location (*3*).

A multiphase research project funded by the Iowa Department of Transportation (Iowa DOT) was undertaken at Iowa State University to develop CMP design methods to prevent uplift failures. This paper presents the results of the second phase in this investigation. In this phase, theoretical relationships were developed for predicting the longitudinal stiffness, yield moment capacity, and ultimate moment capacity of CMP with any corrugation style, strength, and stiffness characteristics. Laboratory tests were conducted on steel pipes (3×1 corrugation style) to experimentally evaluate the accuracy of the theoretical relationships when applied to these specific pipes. Results from the first and third phases of this research project are detailed in the papers by Lohnes et al. and Kjartanson et al. elsewhere in this volume.

B. T. Havens, Woodward-Clyde Consultants, 101 South 108 Ave., Omaha, Nebr. 68154. W. Klaiber and R. A. Lohnes, Department of Civil and Constr. Engr., Iowa State University, Ames, Iowa 50011. L. W. Zachary, Aeronautic Engineering and Engineering Mechanics, Iowa State University, Ames, Iowa 50011.

EXPERIMENTAL WORK

Test Specimens

To address the lack of relevant flexural test information available in the literature, a program of flexural tests of large diameter CMP specimens was initiated. Two test specimens (1.22-m (4-ft) diameter and 1.83-m (6-ft) diameter) were selected for testing. Descriptions of the two test specimens are shown in Table 1. The two specimens in Table 1 will be denoted throughout this document as ISU1 (1.22-m (4-ft) diameter) and ISU2 (1.83-m (6-ft) diameter).

Load Frame

The CMP specimens were simply supported and a uniformly distributed load was applied in increments along the length of the pipe.

Figure 1 is a photograph of ISU1 being tested in the load frame. More details on the load frame are presented in the work of Klaiber et al. (*4*).

As observed in Figure 1, wire rope suspended between upright columns provided end support for the specimens. This type of support facilitated testing various diameters of CMP with minimal adjustments and permitted end rotation. To prevent horizontal movement of the test specimens, brackets that allowed end rotation and vertical deflection were attached to one end of the CMP. Reinforced concrete diaphragms were cast in both ends of the CMP test specimens to add strength and prevent local failure.

Test Procedure

The testing program included a service load test and a failure load test for each specimen. In the service load tests, it was planned to limit applied loading to the elastic range; however, both specimens experienced some plastic deformation in the service load tests. During the failure load tests, each specimen was loaded into the range of plastic deformation until a corrugation collapsed on the compression side of the CMP.

TABLE 1 Flexural Test Specimens

Parameter	ISU1	ISU2
Diameter, m	1.21	1.83
Corrugation style	3 x 1	3 x 1
Fabrication style	Helical Welded Seam	Helical Welded Seam
Nominal length, m	6.10	7.62
Effective length, m	6.01	7.45
Gage	12	14
Nominal uncoated thickness, cm	0.2657	0.1897
Weight, N/m	730	1095

Note: 1 m = 3.28 ft
1 cm = 0.394 in.
1 N/m = 0.0685 lbf/ft

Load was applied to the CMP specimens in predetermined increments with sandbags on top of the pipe and water inside the pipes. Initial increments of loading were applied with uniformly distributed sandbags of known weight. In the failure tests, when additional weight was required, load was applied by adding water inside the specimens. The end concrete diaphragms contained the water in the pipes. By monitoring the depth of water in the specimens, the nonuniform loading (i.e., varying depth of water) was taken into account.

Instrumentation

Each test specimen was instrumented with electrical-resistance strain gauges, direct current displacement transducers (DCDTs), dial gauges, deflection gauges, and manometers. Electrical instrumentation was monitored and recorded after each load increment with a computer-controlled data acquisition system. All other instrumentation was recorded manually after each load increment.

Strain gauges were installed at the centerline of the specimen and at the quarter point sections. At the centerline of the specimens, strain gauges were attached on the top and bottom surface of the CMP as shown in Figure 2. Thus, it was possible to measure longitudinal and hoop strain at the three locations. At the quarter points, strain gauges were positioned on the top and bottom of the specimens so that longitudinal strains could be measured.

DCDTs were positioned longitudinally around the circumference of the CMP, as shown in Figure 3, at the centerline of the specimens to measure movements between corrugation peaks. The DCDTs were attached so that at each location there was a nominal gauge length of 15.24 cm (6 in.). DCDTs were also used to measure changes in the horizontal CMP diameter at the centerline of the specimens as loading was applied.

Vertical deflections of the specimens were determined by reading with surveying levels engineering scales attached to the specimens. This system was used because the expected deflections would exceed the range of the DCDTs available. Vertical deflections were measured at the top and bottom of the specimens at the centerline, and at the bottom of the specimens at quarter point locations. Deflection data at the centerline of the specimens were used to determine changes in the vertical diameter of the specimens.

Dial gauges were used at the ends of the specimens to determine vertical deflections at these locations because of elongation of the wire rope with applied loading. Deflections at quarter points and centerline were adjusted to account for the wire rope elongation.

Manometers were attached to the bottom of the test specimens (quarter points and centerline) to determine the depth of water in the

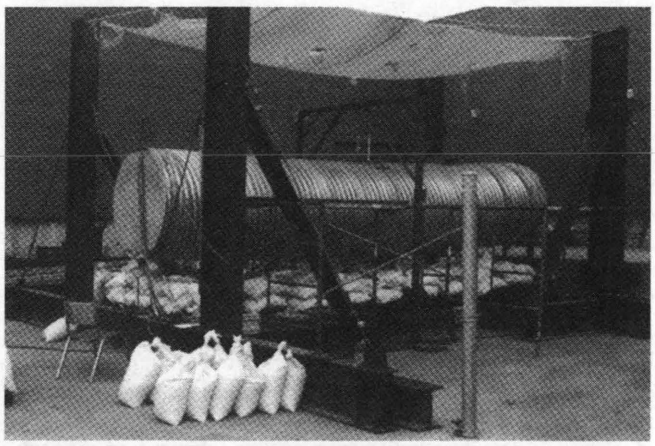

FIGURE 1 Load frame with ISU1 being tested.

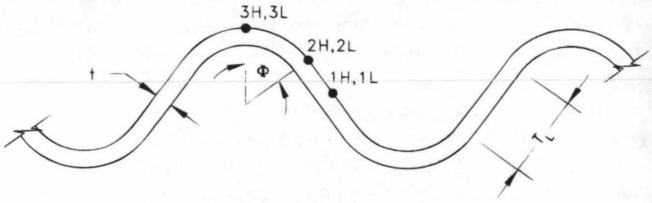

GAUGE	LOCATION	ORIENTATION
1H	INFLECTION POINT	HOOP
1L	INFLECTION POINT	LONGITUDINAL
2H	TANGENT POINT	HOOP
2L	TANGENT POINT	LONGITUDINAL
3H	CREST	HOOP
3L	CREST	LONGITUDINAL

FIGURE 2 Location of centerline strain gauges on top and bottom of CMP.

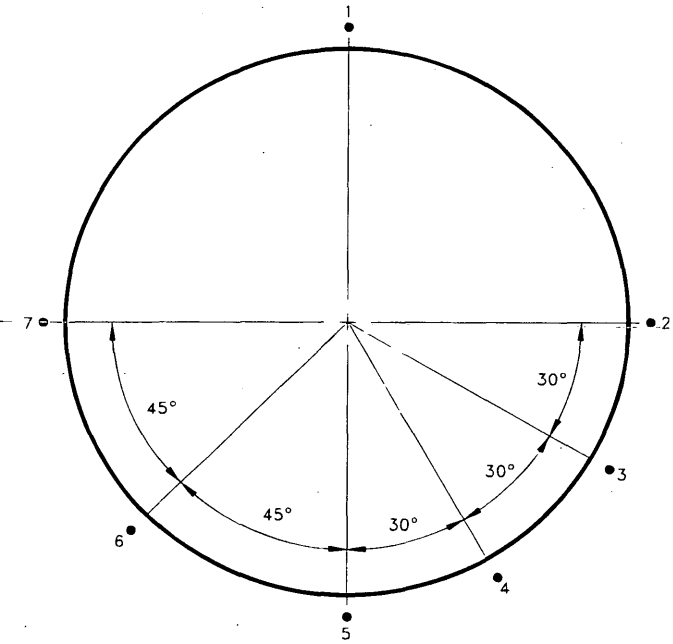

FIGURE 3 Location of DCDTs around circumference of CMP at centerline of span.

CMP specimens at any load increment. With these data, the variation in applied load with deflection of the specimens could be determined.

Experimental Results

The following general observations apply to both specimens; more details can be found in the thesis by Havens (*5*). Strains on the tension side of the specimens were generally smaller than strains measured at the corresponding corrugation positions on the compression side. These strains indicate higher stresses are associated with the collapse of corrugations (top of specimen) than the elongation of corrugations (bottom of specimens). Strain data from the quarter point locations of the specimens indicated symmetrical behavior.

In general, horizontal corrugation crest displacements were proportional to the vertical distance from the CMP neutral axis. Horizontal crest displacements at the top and bottom of the specimens were not always similar values, indicating the possibility of unsymmetrical behavior with respect to the neutral axis of the specimens. Significant changes in the diameters of the specimens occurred depending on the method of load placement.

The relationships between the midspan deflections and the moment for specimens ISU1 and ISU2, respectively, are shown in Figures 4 and 5. In each of these figures, service loading (dashed lines) as well as failure loading (solid lines) are illustrated. The moments at zero deflection are because of the weight of the CMP. The vertical lines at the end of each curve represent the sudden deflections that occur when the specimens reach their ultimate capacity.

The service load data in Figure 4 shows a linear load-deflection curve between Point A and Point B because of sand loading. The curve becomes nonlinear between Point B and Point C because of the non-uniform water loading and an increase in the vertical diameter of the CMP, which causes the measured vertical deflections to increase. Thus, the vertical deflection results from both flexure and localized cross-section deformations. The load-deflection response in the failure test shows a linear curve from Point D to Point C where the loading is all sand. The loading between Point C and Point E is water. At Point E, a load shift occurred when a portion of the sand load fell from the CMP. Although the midspan moment on the CMP decreased, the CMP deflection increased, suggesting that significant plastic deformations of the CMP occurred at or before the instant the load decreased. Points F and G represent the midspan moments because of load remaining on the CMP immediately after the load shift and because of load reapplied to the CMP. Point H is the projected deflection at which the ultimate CMP moment was reached,

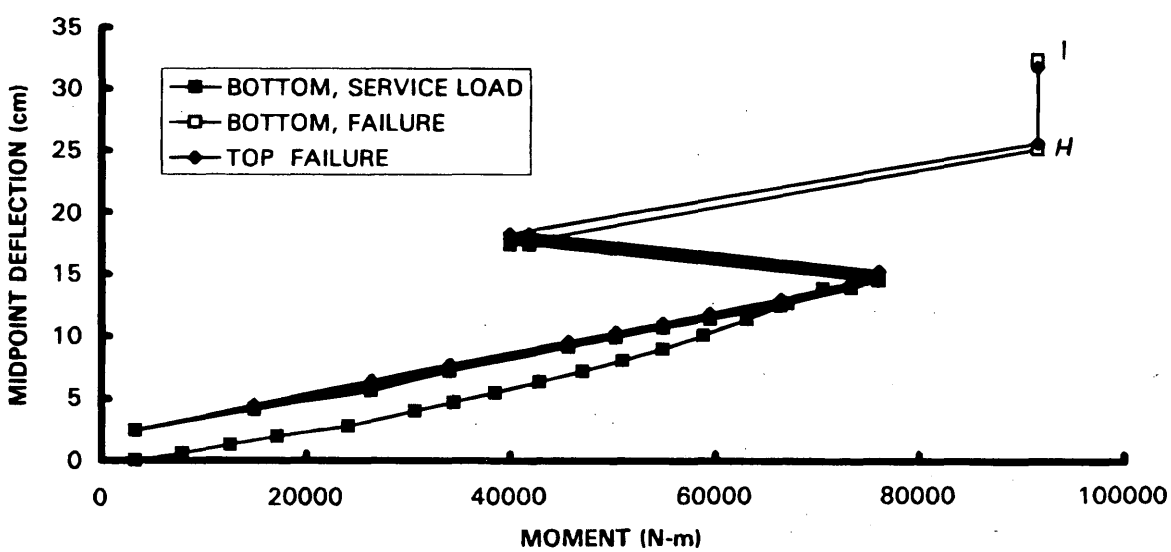

Note: 1 cm = 0.394 in.
1 N-m = 0.737 lbf-ft

FIGURE 4 Moment versus midspan deflection (ISU1).

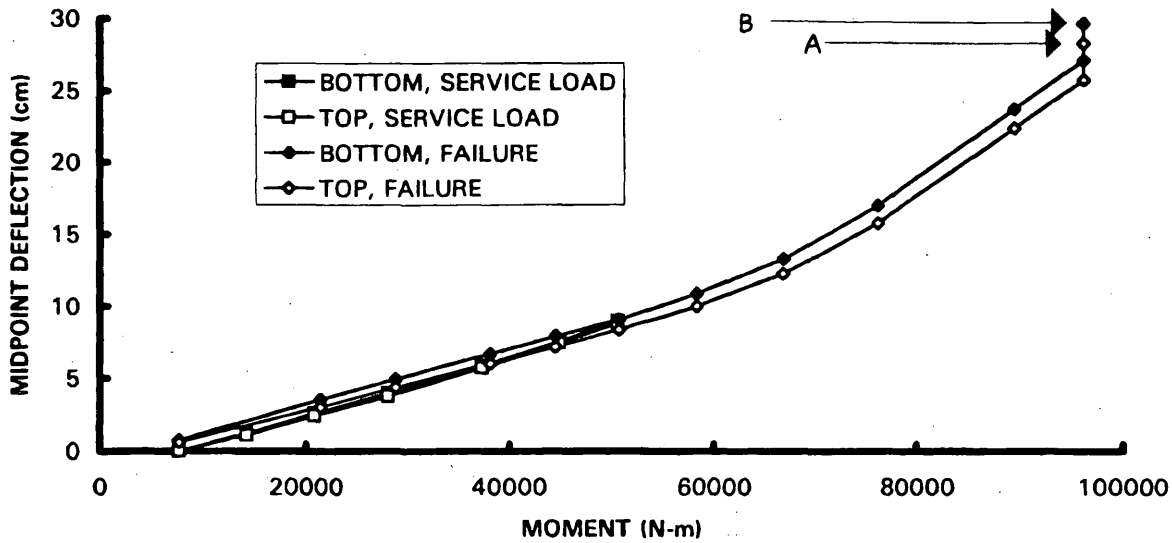

Note: 1 cm = 0.394 in.
1 N-m = 0.737 lbf-ft

FIGURE 5 Moment versus midspan deflection (ISU2).

and Point I is the measured deflection that occurred after the specimen collapsed.

Figure 5 indicates fairly uniform behavior throughout service load and failure tests for ISU2. The primary difference between the deflection curves for service load and failure may be because of the minor plastic deformations that occurred during the service load tests. Points A and B are projected midspan post-collapse deflections. Actual values for those points were not obtained because of failure of the deflection measurement system.

Corrugations in ISU1 collapsed at a distance of 10.16 to 12.70 cm (4 to 5 in.) from the centerline. Corrugations collapsed in ISU2 at two locations. One collapse occurred at a welded seam approximately 33.02 cm (13 in.) from the centerline and the other collapse occurred approximately 1.12 m (44 in.) from the midspan on the opposite half of the span. The second collapse followed the first by approximately 20 to 30 sec.

Longitudinal moment capacities, stiffness values, and midspan deflections from test data are summarized in Table 2. In this table, yield moments are taken as those moments occurring when the relationship between the longitudinal strain at the corrugation crest and the applied moment becomes nonlinear. A range is given for the yield moment for ISU2 as it was difficult to identify the actual point. Midspan yield deflections for ISU2 are also presented as a range. Ultimate moments were reached when the corrugation under the greatest strain collapsed. At this magnitude, the specimen could not carry additional load without excessive, unpredictable deflection.

TABLE 2 Experimental Test Results

	Specimen	
Parameter	ISU1	ISU2
Yield Moment, kN-m	30.7	28.1-37.3
Ultimate Moment, kN-m	91.5	96.3
EI, MN-m^2	2.49	2.61
Mid-span Defl., cm @ yield moment	3.81	3.81-5.84[b]
Mid-span Defl., cm @ ult. moment	<13.7[c]	>27.2[c]

[a] difficult to interpret a single value for location of non-linear behavior; range is used
[b] deflections in the range of interpreted yield moment
[c] unable to measure deflection at instant of incipient collapse

Note: 1 kN-m = 737 lbf-ft
1 MN-m^2 = 2.42 x 10^6 lbf-ft^2
1 cm = 0.394 in.

Maximum deflection values are reported just before the large deflection associated with corrugation collapse. For both specimens, the ultimate moment was reached between load increments, so the deflection under ultimate moment was not measured and is indicated as a value greater than the measured deflection at the previous load increment.

Values of stiffness (EI) in Table 2 were calculated from the service load test assuming that each simple-span CMP specimen was subjected to uniform distributed loading. This was an appropriate assumption for ISU1 in which only sandbag loading was used in the service load test. For ISU2 in which water loading was used in the service load test, corrections were required for non-uniform loading. Basic load deformation relationships were used to determine the EI values from the experimental data.

The modulus of elasticity of the steel was assumed to be the commonly accepted value of 200 MPa (29×10^6 psi). Poisson's ratio, ν, for steel was taken as 0.3.

The ratios of hoop strains, ϵ_H, to longitudinal strains, ϵ_L, were calculated for each test at two locations on the top of the CMP specimens. Strain ratios were used to calculate the stress ratio, K_σ, which is the ratio of hoop stress to longitudinal stress. From test data, the average strain ratio was found to be 0.38. The stress ratio, K_σ, can be written as indicated below:

$$K_\sigma = \frac{\sigma_H}{\sigma_L} = \frac{\left(\frac{\epsilon_H}{\epsilon_L}\right) + \upsilon}{\left[\left(\frac{\epsilon_H}{\epsilon_L}\right)\upsilon\right] + 1} \tag{1}$$

where

ϵ_L is the longitudinal strain,
ϵ_H is the hoop strain, and
ν is Poisson's ratio.

Using the strain ratio of 0.38 and Equation 1, the stress ratio, K_σ, is found to be 0.64 for 3×1 pipe.

THEORETICAL DEVELOPMENT

Theoretical Longitudinal Moment Capacity

Based on the principles of mechanics, observations, and data from the flexural tests, relationships were developed for calculating the longitudinal moment capacity of CMP.

A free body diagram of the quarter cycle indicated in Figure 6 is at the critically stressed location in the transverse section. In Figure 6(*b*), dP and $dP + d\,(dp/dx)$ are the compressive forces acting on the ends of the corrugation. The moment, M_c, is the local moment on the corrugation. Forces F_{H1} and F_{H2} are the forces acting on the sides of this longitudinal section resulting from hoop stresses that are resisted by the force, V.

In the development of a relationship for the CMP moment, M_E, the following assumptions are made:

- Hoop strains at the inflection point that are typically small are assumed to be zero;
- Hoop and longitudinal strains are assumed to vary linearly with the distance from the corrugation neutral axis (CNA) indicated in Figure 6(*b*); and
- Force, dP, is assumed to vary from a maximum at the top of the CMP to zero at the CMP neutral axis.

The stresses on this element are related to the applied forces and moments on the element by using the principles of mechanics. For details on this development, the reader is referred to the work of Klaiber et al. (*6*). The CMP moment, M_E, because of a specified limiting stress, may be expressed as:

$$M_E = \frac{2\pi r\, t\sigma_L}{d_c}\left[\frac{rt}{6} + K\sigma\left(\frac{L_T^2 \cos\phi}{12} R_{TP} + K_\lambda R\right)\right] \tag{2}$$

where

σ_L signifies a limiting longitudinal stress within the elastic range;
K_σ is the ratio of hoop stress to longitudinal stress for any CMP element;
d_c is the corrugation depth indicated in Figure 6(*a*);
r is the CMP radius;
t is the CMP wall thickness;
L_T is the length of the tangent section in each corrugation cycle as indicated in Figure 6(*a*);
ϕ is the tangent angle indicated in Figure 6(*a*);
R_{TP} is ratio of the distance from the CNA to the tangent point to the distance from the CNA to the crest of the corrugation;
K_λ is a constant that depends on the corrugation geometry; the average value for all pipe gauges may be taken as 0.3828 in. for 3×1 CMP, 0.2174 in. for $2\frac{2}{3} \times \frac{1}{2}$ CMP, and 0.2124 in. for $2 \times \frac{1}{2}$ CMP; values for specific gauges may be calculated using relationships presented in the work of Havens (*5*); and
R is the corrugation radius.

Theoretical Longitudinal Ultimate Moment Capacity

Flexural failure of CMP has been defined at a limiting biaxial yield stress on the critical compression-side corrugation. However, considerable moment capacity may exist before the onset of corrugation collapse and severe vertical deflection of the CMP. A formula was developed to calculate this ultimate moment capacity based in part on the previously developed relationship for M_E.

To estimate the ultimate moment capacity from the test data (strains), it was determined that the critically stressed element on the compression side of the CMP had yielded and a plastic hinge formed as more load was applied. This plastic hinge begins at the crest and extends down to the tangent point at incipient collapse. Although a portion of the CMP section yields, other regions of the CMP cross-section behave elastically. An angle designated as θ_{EP}, as indicated in Figure 7, divides the two assumed regions of elastic behavior and plastic behavior. The resisting moment capacity of the elastic region is a modification of the formula developed for determining the limiting stress moment capacity. The resisting moment capacity of the elastic regions and that of the plastic regions is as follows:

$$M_{E(\theta EP)} = \frac{8r\, t\sigma_L}{d_c \cos\theta_{EP}}\left[\frac{rt}{6} + K_\sigma\left(\frac{L_T^2 \cos\phi}{12} R_{TP} + K_\lambda R\right)\right] \times \left[\frac{\pi}{4} - \frac{\theta_{EP}}{2} - \frac{\sin 2\theta_{EP}}{4}\right] \tag{3}$$

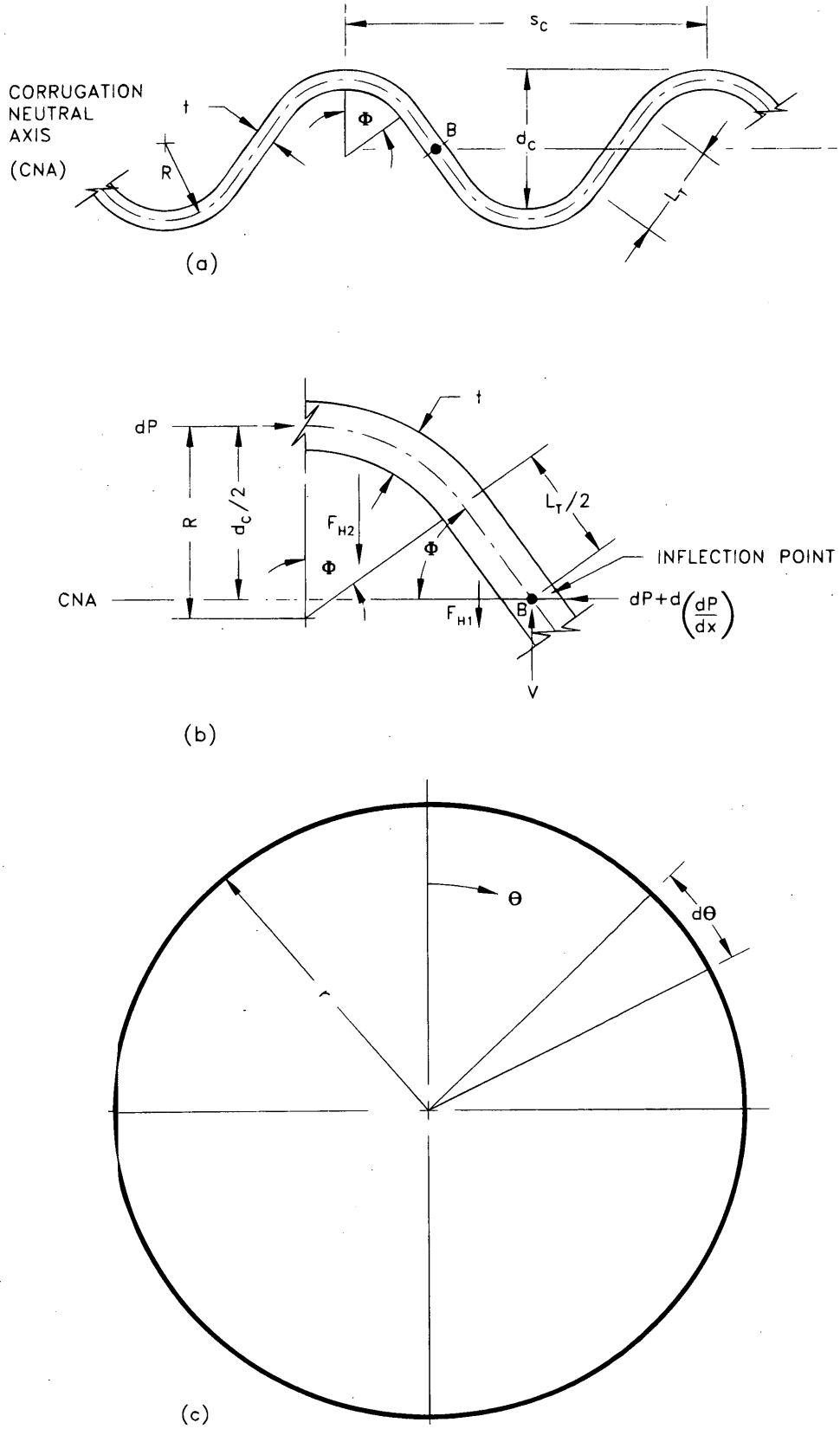

FIGURE 6 Description of CMP: (a) corrugation details; (b) free body diagram of one-quarter corrugation cycle; (c) transverse cross section.

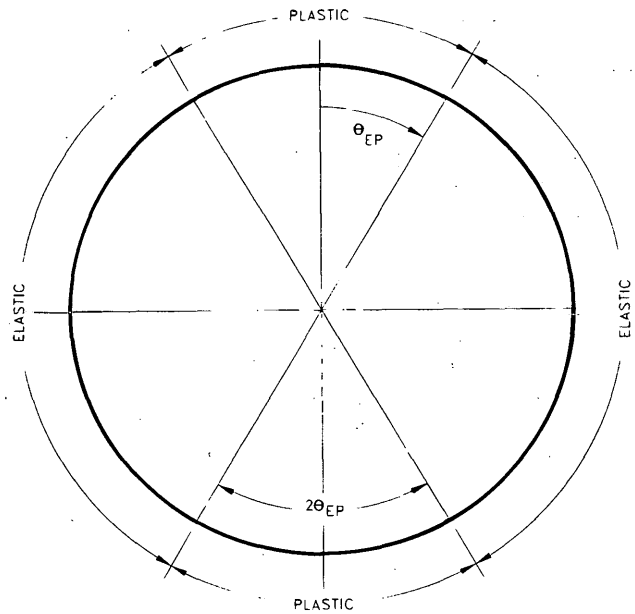

FIGURE 7 Assumed elastic and plastic regions of CMP at ultimate flexural strength.

where $M_{E(\theta EP)}$ is the elastic region moment contribution to the ultimate moment.

$$M_{P(\theta EP)} = \frac{4\sigma_{YL} rt}{\sin\phi}\left[K_\sigma\left(R\phi\frac{L_T}{6}\right)\cos\phi + \frac{rt}{2L_T}\right]\sin\theta_{EP} \quad (4)$$

where $M_{P(\theta EP)}$ is the ultimate moment contribution from the plastic region. The ultimate moment based on θ_{EP} is the sum of the resisting moments from the two previous relationships:

$$M_{U(\theta EP)} = M_{P(\theta EP)} + M_{E(\theta EP)} \quad (5)$$

Using the ultimate moments obtained from the tests and the previously determined value of 0.64 for K_σ, a value for θ_{EP} was calculated to be 73.4 degrees. The contribution to the moment capacity from the elastic part of the cross-section is small, however, in comparison to the contribution from the plastic part of the cross-section. With the assumption that the entire cross-section is subjected to plastic deformation (θ_{EP} = 90 degrees), the ultimate moment capacity simplifies to the following relationship:

$$M_u = \frac{4\sigma_{YL} rt}{\sin\phi}\left[K_\sigma\left(R\phi + \frac{L_T}{6}\right)\cos\phi + \frac{rt}{2L_T}\right] \quad (6)$$

Theoretical EI Factor

In order to calculate CMP vertical deflections, an EI term is required. Moment of inertia, I, is a function of the CMP geometry; however, the calculation of I for CMP is complex because the CMP transverse cross-section is not constant in the longitudinal direction. The moment of inertia for CMP is considerably smaller than the I of a smooth-wall pipe ($I = \pi r^3 t$), because the smooth wall has a constant transverse cross-section which is much stiffer.

To develop an expression for I, an energy approach was used to determine a relationship between the applied load and the CMP midspan vertical deflection. Several assumptions were made about the distribution of stresses throughout the CMP. Loading is assumed to produce a moment on the CMP such that the critically stressed element on the compression side of the CMP is at a specified limiting stress within the elastic range. All other elements in the CMP are assumed to be at stress levels lower than the limiting stress. Stresses at these other locations are quantified to account for variables such as position of element in span, relationship of element to CNA, and relationship of element to CMP neutral axis. Strain energy imparted to the CMP specimen by the applied loads is related to the elemental stresses as follows:

$$U = 2\sum_{n=1}^{N_R}\int\left(\frac{\sigma_{P1}^2}{2E} + \frac{\sigma_{P2}^2}{2E}\right)dV \quad (7)$$

where $ds = rd\theta$, $dV = rd\theta dtdx$, N_R is the number of quarter-cycle segments in one-half of the CMP length, n is the quarter-cycle segment count number used in the summation, and σ_{P1} and σ_{P2} are the principal stresses on each element. The strain energy is then related to deflection of the CMP specimen as follows:

$$\frac{\partial U}{\partial P} = \Delta_V = \left[\frac{4\sigma_{MAX}^2 rK_G\pi t}{EM_{MAX}^2 d_c^2}\right]\left(\frac{1}{3} + K_\sigma^2\right)\sum_{n=1}^{N_R} 2M_x \quad (8)$$

where M_x is the moment at a distance x from the end. From beam theory, the EI factor is then related to the applied moment and limiting stress as follows:

$$EI = \frac{s_c}{4}\left[\frac{M_{MAX}^2 Ed_c^2}{4\sigma_{MAX}^2 rK_G\pi t}\right]\left[\frac{3}{1+3K_\sigma^2}\right] \quad (9)$$

Incorporating Equation 2, the following relationship for EI is determined:

$$EI = \frac{E\pi s_c rt}{4K_G}\left[\frac{3}{1+3K_\sigma^2}\right]\left[\frac{rt}{6} + K_\sigma\left(\frac{L_T^3\sin\phi\cos\phi}{12d_c} + K_\lambda R\right)\right]^2 \quad (10)$$

where, except for K_G and s_c, all terms have been previously defined. K_G is a geometric parameter which may be taken as 0.09215 in.^{3} for 3 × 1 CMP, 0.01928 in.^{3} for 2⅔ × ½ CMP, and 0.01388 in.^{3} for 2 × ½ CMP; note that these values are averages for all common pipe gauges. Values for specific gauges may be calculated using relationships presented in the work of Havens (*5*). The corrugation crest spacing (length of one cycle) is denoted as s_c.

Application of Theoretical Relationships

The theoretical relationships were developed for use with CMP of any metal type and any corrugation style consisting of circular arcs connected by tangents. Most of the parameters needed for application of the relationships can be determined theoretically. However, the stress ratio (K_σ) must be determined experimentally for specific corrugation styles. The relationships in this paper are validated only with test data from 3 × 1 CMP.

Helix Angle Effects on Strength and Stiffness

The helix angle of CMP varies from approximately 33 degrees for small diameter pipes to 6 degrees for large diameter pipes, with

variations resulting from corrugation style and manufacturer. It was postulated by Lane (*6*) that CMP with helix angles less than 8 degrees will act similar to CMP with annular corrugations. The relationships developed for longitudinal moment capacity and stiffness assume circumferential corrugations. This assumption is expected to be reasonable for the larger diameter pipes tested as part of the ISU study, but may not be valid when the theoretical formulas are applied to smaller diameter pipes, where the helix angle may be related to substantial increases in stiffness. Neglecting the helix angle effects should be conservative, as the beam strength of helical pipe of equal size and gauge is greater than that of annular CMP because of the diagonal direction of the corrugations (*7*).

Comparison of Experimental and Theoretical Results

Experimental results and theoretical values calculated from Equations 2, 6, and 10 are shown in Table 3. Equation 2 predicts nonconservative yield moments which are 11.5 percent high for ISU1 and 3.6 to 37.7 percent high for ISU2. The main reasons for this difference are that it is very difficult to determine the yield moment experimentally and the variation in yield stress from specimen to specimen. Values calculated for the ultimate moments from Equation 6 are in excellent agreement with the experimental values being 1.5 percent low for ISU1 and 4.2 percent high for ISU2. Recall, however, that the theoretical values are based on an assumption that the entire cross section is yielding.

Values for *EI* determined by using Equation 10 are in reasonable agreement with the experimental values. The theoretical values of EI are 4.3 percent low and 8.1 percent high for ISU1 and ISU2, respectively.

SUMMARY AND CONCLUSIONS

Presented in this paper are the results of one phase of an ongoing investigation whose overall objective is to determine when restraint is required to prevent uplift failures in CMP. In this phase of the study, three CMPs were loaded to failure to determine experimental values for yield moments, ultimate moments, and "stiffness" *EI*.

Theoretical relationships were derived for determining the yield moment, ultimate moment, and the "stiffness" *EI* for CMPs of various diameters, gauges, and corrugation geometry. The theoretical relationship for yield moments from Equation 2 provides slightly unconservative values. Variation in the yield strength of steel is believed to be the main reason for the difference. Theoretical ultimate moment capacities obtained using Equation 6 are in good agreement with the values that were obtained experimentally. The relationship for "stiffness" *EI*, Equation 10, provides values that are in good agreement with the experimental values determined.

ACKNOWLEDGMENTS

The research presented in this paper was conducted by the Engineering Research Institute of Iowa State University, and was funded by the Highway Research Board and the Highway Division, Iowa DOT, Ames, Iowa. The authors wish to thank various engineers from the Iowa DOT, especially D.D. Coy for his support, encouragement, and counseling. Appreciation is also extended to R.L. Meinzer of Contech Construction Products, Inc., Topeka, Kansas, for donating the numerous sections of CMP used in the tests. Special thanks are also accorded the numerous undergraduate students who assisted with the various phases of the project.

TABLE 3 Comparison of Experimental and Theoretical Values

	ISU1	ISU2
Experimental Yield Moment, kN-m	30.7	28.1 to 37.3
Theoretical Yield Moment, kN-m	34.2	38.7
Difference from experimental value (%)	+11.5	+3.6 to +37.7
Experimental Ultimate Moment, kN-m	91.5	96.3
Theoretical Yield Moment, kN-m	90.2	100
Difference from experimental value (%)	-1.5	+4.2
Experimental EI Factor, MN-m^2	2.49	2.61
Theoretical EI Factor, MN-m^2	2.39	2.83
Difference from experimental value (%)	-4.3	+8.1

Note: 1 kN-m = 737 lbf-ft
1 MN-m^2 = 2.42 x 10^6 lbf-ft^2

REFERENCES

1. *Pipe Culvert Inlet and Outlet Protection.* Notice N 5040.3. FHWA, U.S. Department of Transportation, April 26, 1974.
2. Edgerton, R. C. Culvert Inlet Failures-A Case History. *Highway Research Board Bulletin 286*, 1960, pp. 13–21.
3. Pestotnik, C. *Report on Flexible Culvert Inlet Flotation Failures Survey.* Letter to County Engineers, Iowa DOT Ref. No. 521.1, Feb. 20, 1976.
4. Klaiber, F. W., R. A. Lohnes, L. W. Zachary, T. A. Austin, B. T. Havens, and B. T. McCurnin. *Design Methodology for Corrugated Metal Pipe Tiedowns: Phase I.* Final Report ISU-ERI-Ames-93409, Engineering Research Institute, Iowa State University, Ames, Iowa, 1993, 181 pp.
5. Havens, B. T. *Determination of the Longitudinal Strength and Stiffness of Corrugated Metal Pipe.* M.S. thesis, Iowa State University, Ames, Iowa, 1993.
6. Lane, W. W. *Comparative Studies on Corrugated Metal Culvert Pipes.* Report No. EES-236, Engineering Experiment Station, Ohio State University, Feb. 1965.
7. Armco Drainage and Metal Products. *Handbook of Drainage and Construction Products.* Armco, Middletown, Ohio, 1955.

The opinions, findings, and conclusions expressed herein are those of the authors and not necessarily those of the Iowa DOT or the Highway Research Board.

Publication of this paper sponsored by Committee on Culverts and Hydraulic Structures.